Computational Mechanics
https://doi.org/10.1007/s00466-018-1617-2

ORIGINAL PAPER

Modeling the spatio-thermal fire hazard distribution of incandescent material ejecta in manufacturing

T. I. Zohdi[1]

Received: 1 May 2018 / Accepted: 31 July 2018

Abstract

A mathematical model is developed to characterize the progressive time-evolution of a fragmenting incandescent object. The objective of these models is to provide a spatio-thermal footprint of the fragmentation field, which can be useful to guide fire safety rules in manufacturing workplaces, as well as to estimate fire hazards. Ascertaining the time-evolution of the temperature of the fragments is quite difficult to measure experimentally, which motivates the model development. Initially, analytical models based solely on ballistics, which provide qualitative trends, are developed to provide insight into the fundamental ratios that govern safe operating conditions. Thereafter, rapid numerical spatio-thermal models, which provide quantitative information, are then developed, based on particle methods. The model uses the released energy from the initial blast pulse to provide the starting kinetic energy of the system of particles and then numerically computes the trajectory and thermal state of the fragments under the influence of

- drag from the surrounding air,
- gravitational settling and
- convective and radiative cooling.

Numerical examples and provided and extensions to high-fidelity are discussed.

Keywords Fragmentation · Spatio-thermal footprint · Convection · Radiation

1 Introduction

The start of unwanted fires by the ignition of incandescent metallic or ceramic fragments from man-made causes, such as manufacturing workplaces, is a source of growing concern in arid and semi-arid environments, where population growth has been unabated. Oftentimes, such fragments are generated by manufacturing processes involving, cutting, grinding, sanding, welding, etc, as well as metal-to-metal contact from construction sites, worn-out brakes, vehicles exhaust systems, ballistic impacts, explosions, pyrotechnics, etc. Also, situations involving clashing power lines in high winds, leading to hot charged material being ejected are of concern (Fig. 1). The generation of such incandescent particles is well-documented (Wingerden et al. [1] and Fernandez-Pello [2]). According to the National Interagency Fire Center, from 2006–2015, the average number of wildfires in the United States was 71,594, with nearly seven million acres burnt annually (NIFC report [3]). Depending on the thermal state of the particles and the material on which they land, they can be an source of ignition. There have been many fires that have been attributed to hot metal particles and sparks. Published data (Prestemon et al. [4], Ahrens [5] and Ramljak [6]) indicates that powerlines, machinery and vehicles cause approximately 28,000 natural fuel fires annually in the United States (Aherns [5], NFPA [7] and USFA [8]). These processes depend on many factors, including the thermal state and trajectories of the particles. The scientific significance on understanding this phenomena is that it can potentially save lives and reduce fire damage, for example by ascertaining clearance distances along highways and railroads needed to reduce the likelihood of spot fire initiation. This type of information can help construct safety

✉ T. I. Zohdi
zohdi@me.berkeley.edu

1 Department of Mechanical Engineering 6195 Etcheverry Hall, University of California, Berkeley, CA 94720-1740, USA

Fig. 1 Examples of spot ignition generation in manufacturing (see public domain photos: https://www.pexels.com/public-domain-images/)

regulations. The subject of spot ignition by metal particles involves number of parameters. Early studies on the subject were primarily experimental (Pleasance and Hart [9], Stokes [10] and Rowntree and Stokes [11]). Fernandez-Pello and co-workers (Hadden et al. [12] and Urban et al. [13]) have investigated the problem in order to better understand the physical/chemical mechanisms controlling the spot fire ignition process (Fernandez-Pello [2]). Experimental tests are, however, quite expensive and time consuming. For example, the usual experimental approach is to heat a particle of a metal usually encountered in spot fires (typically, steel, aluminum, copper, brass), which is then dropped onto a fuel bed of interest, in order to ascertain if ignition will occur. The more complex test problem of the interaction with wind, airborne cooling, etc, is experimentally daunting. This motivates the work presented in this paper. Specifically, a mathematical model is developed to characterize the progressive time-evolution of an incandescent object that fragments into multiple pieces. The objective of this model is to provide a spatio-thermal footprint of the fragmentation field, which can be useful to guide fire safety rules in manufacturing workplaces, as well as to estimate fire hazards. Ascertaining the time-evolution of the temperature of the fragments is extremely difficult to measure in experiments, thus motivating the development of the model. A direct numerical scheme based on particle dynamics is constructed. The model uses the released energy from the initial blast pulse to provide the starting kinetic energy of the system of particles and then numerically computes the trajectory and thermal state of the fragments under the influence of

- drag from the surrounding air,
- gravitational settling and
- convective and radiative cooling.

Initially, analytical models based solely on ballistics, which provide qualitative trends are developed. These provide insight into the fundamental ratios that govern safe areas in a spatio-thermal map. Thereafter, a rapid numerical spatio-thermal model, which provides quantitative information, is then developed. Finally, extensions to high-fidelity are discussed.

Remark 1 We restrict ourselves to the initial stages of a complex process, namely the generation and ballistic trajectory of hot metallic/ceramic incandescent particles. The subsequent phenomena of burning embers after these fragments have made contact with a combustible surface is outside the scope of the present work, as is the problem of burning embers lofted in a fire plume and/or transported by ambient winds. We refer the reader to works dedicated to correlations or CFD simulations found in Baum and McCaffrey [14] and Tarifa [15]. The launching of embers by ground fires has been investigated by many researchers, with pioneering work conducted by Tarifa et al. [15,16], who experimentally determined drag and burning rates of spheres, cylinders and plates of various woods, and then ascertained the maximum fire spread range. This was followed by a large number of theoretical and experimental studies of ember transport (Sardoy et al [17], Lee et al. [18] and Koo et al. [19], Pleasance and Hart [9], Tse and Fernandez-Pello [20], Mills and Hang [21], Tarifa et al. [16] and Rallis and Mangaya [22]).

Remark 2 We emphasize that there are different ways for incandescent metallic particles to be generated. One unique way is by power line (generally aluminum or copper) interactions in high-winds (referred to as buffeting or galloping) which arc or clash (Pleasance and Hart [9], Russell et al. [23] and Blackburn [24], Badger [28]). In such situations, metal fragments may be produced and ejected from the arcing location (Pagni [25], Gilbert [26], Maraghides and Mell [27] and Ramljak et al. [6] and Pleasance and Hart [9]).

2 General assumptions

We will study a model problem comprised of a mass which explodes, producing blast fragments that are quite small and moving radially-outwards. The amount of rotation contributes negligibly to the overall trajectory of the fragments. We assume that upon detonation, each fragment has the same impulsive velocity [denoted $\delta \boldsymbol{v}(0)$], in the radial direction from the center of the blast (consistent with camera observations in Zohdi and Cabalo [54]). The mass of the explosive material is considered negligible and is converted to energy, which is imparted to the surrounding fragmenting material. Thus, mathematically, the velocity vector pulse is radially-outward from the center of the sphere, co-located at the center of mass of the explosive material:

$$\delta \boldsymbol{v}_i(0) = ||\delta \boldsymbol{v}(0)|| \left(\frac{\boldsymbol{r}_i(0) - \boldsymbol{r}_c(0)}{||\boldsymbol{r}_i(0) - \boldsymbol{r}_c(0)||} \right) \stackrel{\text{def}}{=} ||\delta \boldsymbol{v}(0)|| \boldsymbol{n}_{ri} \quad (2.1)$$

where $\boldsymbol{r}_i$ is the position vector of the ith fragment, $\boldsymbol{n}_{ri}$ is the normal/radial direction and

$$\boldsymbol{r}_c(0) = \frac{1}{\left(\sum_{i=1}^{N} m_i\right)} \sum_{i=1}^{N} m_i \boldsymbol{r}_i(0), \quad (2.2)$$

where N is the number of fragments, $\boldsymbol{r}_c(0)$ is the center of mass of the fragmenting material and m_i is the mass of each fragment. *A non-interaction assumption is appropriate since all of the fragments are propagating radially-outwards with the same initial velocity, thus, the inter-fragment collisions are negligible. This assumption is discussed further in the paper.* We further assume. that the magnitude of the initial velocity pulse dictates initial energy released (E), which is assumed to be converted into kinetic energy for the material at ($t = 0$):

$$E = \sum_{i=1}^{N} \frac{1}{2} m_i ||\delta \boldsymbol{v}(0)||^2 \Rightarrow ||\delta \boldsymbol{v}(0)|| = \sqrt{\frac{2E}{\sum_{i=1}^{N} m_i}} = \sqrt{\frac{2E}{M}}, \quad (2.3)$$

where $\delta \boldsymbol{v}(0)$ is the velocity of pulse imparted to a fragment in the radial direction, M is the total detonation material mass, $m_i = \rho_i \frac{4}{3} \pi R_i^3$ is mass of the individual fragments, where ρ_i is the density of the fragments. Finally, we assume that the velocity of the surrounding medium ($\boldsymbol{v}^f$) is given and is unaffected by the fragments.[1]

Remark In the general case where the object was moving before the blast, the pulse velocities can be added to the velocity vectors immediately before the pulse ($\boldsymbol{v}^-(0)$)

$$\boldsymbol{v}_i^+(0) = \boldsymbol{v}_i^-(0) + \delta \boldsymbol{v}_i(0). \quad (2.4)$$

We neglect any interaction between a possible explosive shock wave and the fragments. This is discussed further later in the paper.

[1] We will discuss this assumption later in the paper.

3 Approximate analytical solutions and trends

In addition to the previous assumptions, we also assume spherical fragments with varying radii (R_i, $i = 1, 2, 3 \ldots N = fragments$) and:

- For the fragments, the effects of their rotation with respect to their mass center are unimportant to their overall motion, yielding the simple following equation of motion for the ith fragment

  $$m_i \dot{\boldsymbol{v}}_i = \boldsymbol{\Psi}_i^{grav}, \quad (3.1)$$

  with initial velocity $\boldsymbol{v}_i(0)$ and initial position $\boldsymbol{r}_i(0)$. The gravitational force is $\boldsymbol{\Psi}_i^{grav} = m_i \boldsymbol{g}$, where $\boldsymbol{g} = (g_x, g_y, g_z) = (0, 0, -9.81)$ m/s^2.
- For the thermal state of the fragments ($\theta_i' s$), from the First Law of Thermodynamics:

  $$m_i C_i \dot{\theta} = h_i (\theta_e - \theta_i) A_i^s, \quad (3.2)$$

  where C_i is the heat capacity, h_i is the convection coefficient, θ_e is the surrounding temperature and $A_i^s = 4\pi R_i^2$.

The effects of drag are neglected in this section.

3.1 Simple ballistic calculation

In the vertical z-direction, ignoring everything except for gravity yields for each particle

$$v_{iz}(t) = v_{iz}(0) - gt \Rightarrow t = \frac{v_{iz}(0)}{g}, \quad (3.3)$$

which provides the time going up (to $v_{iz}(t) = 0$, stage I)

$$t_1 = \frac{v_{iz}(0)}{g} \quad (3.4)$$

and coming down

$$t_2 = \sqrt{\frac{2(r_{iz}^{max} - r_{iz}^{min})}{g}}, \quad (3.5)$$

where $r_{iz}^{max} = r_{iz}(t_1)$ and r_{iz}^{min} is the z position of the surface. Going up, from initial launch is given by

$$r_{iz}(t) = r_{iz}(0) + v_{iz}(0)t - \frac{1}{2}gt^2. \tag{3.6}$$

Plugging in t_1 yields

$$\begin{aligned} r_{iz}^{max} &= r_{iz}(0) + v_{iz}(0)\left(\frac{v_{iz}(0)}{g}\right) - \frac{1}{2}g\left(\frac{v_{iz}(0)}{g}\right)^2 \\ &= r_{iz}(0) + \frac{(v_{iz}(0))^2}{2g} \end{aligned} \tag{3.7}$$

Going down, stage II, yields

$$r_{iz}(t) = r_{iz}^{max} - \frac{1}{2}gt^2. \tag{3.8}$$

Setting, $r_{iz}(t_2) = r_{iz}^{min}$ yields

$$t_2 = \sqrt{2\frac{r_{iz}^{max} - r_{iz}^{min}}{g}} = \sqrt{2\frac{r_{iz}(0) - r_{iz}^{min}}{g} + \frac{(v_{iz}(0))^2}{g^2}} \tag{3.9}$$

The total time airborne becomes

$$\begin{aligned} t^{tot} = t_1 + t_2 = \frac{v_{iz}(0)}{g} \\ + \sqrt{2\frac{r_{iz}(0) - r_{iz}^{min}}{g} + \frac{(v_{iz}(0))^2}{g^2}} \end{aligned} \tag{3.10}$$

The horizontal distance in-plane distance is given by

$$\begin{aligned} r_{ix}(t^{tot}) = r_{ix}(0) + v_{ix}(0)t^{tot} = r_{ix}(0) \\ + v_{ix}(0)\left(\frac{v_{iz}(0)}{g} + \sqrt{2(\frac{r_{iz}(0) - r_{iz}^{min}}{g}) + \frac{(v_{iz}(0))^2}{g^2}}\right) \end{aligned} \tag{3.11}$$

3.2 Simple thermal calculation

Ignoring everything except for convective cooling

$$m_i C_i \dot{\theta} = h_i A_i^s(\theta_e - \theta_i), \tag{3.12}$$

which yields

$$\theta_i(t) = (\theta_i(0) - \theta_e)e^{-\frac{h_i A_i}{m_i C_i}t} + \theta_e \tag{3.13}$$

Plugging in the time yields

$$\begin{aligned} \theta_i(t^{tot}) &= (\theta_i(0) - \theta_e)e^{-\frac{h_i A_i^s}{m_i C_i}t^{tot}} + \theta_e \\ &= (\theta_i(0) - \theta_e)e^{-\frac{h_i A_i^s}{m_i C_i}\left(\frac{v_{iz}(0)}{g} + \sqrt{2\left(\frac{r_{iz}(0) - r_{iz}^{min}}{g}\right) + \frac{(v_{iz}(0))^2}{g^2}}\right)} + \theta_e \end{aligned} \tag{3.14}$$

3.3 Analytical summary

In summary, the analytical expressions are:

- The spread of particles is given by

$$\begin{aligned} r_{ix}(t^{tot}) = r_{ix}(0) + v_{ix}(0)\left(\frac{v_{iz}(0)}{g}\right. \\ \left. + \sqrt{2\left(\frac{r_{iz}(0) - r_{iz}^{min}}{g}\right) + \frac{(v_{iz}(0))^2}{g^2}}\right) \end{aligned} \tag{3.15}$$

- The temperature of the particles at the maximum landing distance is given by

$$\begin{aligned} \theta_i(t^{tot}) &= (\theta_i(0) - \theta_e) \\ &\times e^{-\frac{hA}{m_i C_i}\left(\frac{v_{iz}(0)}{g} + \sqrt{2\left(\frac{r_{iz}(0) - r_{iz}^{min}}{g}\right) + \frac{(v_{iz}(0))^2}{g^2}}\right)} + \theta_e \end{aligned} \tag{3.16}$$

3.4 Key ratio: cooling time to flight time

The ratio of time it takes for a hot fragment to cool to a safe temperature to the time it remains airborne (t^{tot}) is a key.

From expression

$$\theta^{safe} = \theta_i(t^{safe}) = (\theta_i(0) - \theta_e)e^{-\frac{h_i A_i^s}{m_i C_i}t^{safe}} + \theta_e, \tag{3.17}$$

yields

$$t^{safe} = -\frac{m_i C_i}{h_i A_i^s} Ln\left(\frac{\theta^{safe} - \theta_e}{\theta_i(0) - \theta_e}\right). \tag{3.18}$$

The ratio is therefore,

$$\begin{aligned} S \stackrel{\text{def}}{=} \frac{time\ to\ cool}{time\ airborne} = \frac{t^{safe}}{t^{tot}} \\ = \frac{-\frac{m_i C_i}{h_i A_i^s} Ln\left(\frac{\theta^{safe} - \theta_e}{\theta_i(0) - \theta_e}\right)}{\frac{v_{iz}(0)}{g} + \sqrt{2\left(\frac{r_{iz}(0) - r_{iz}^{min}}{g}\right) + \frac{(v_{iz}(0))^2}{g^2}}}. \end{aligned} \tag{3.19}$$

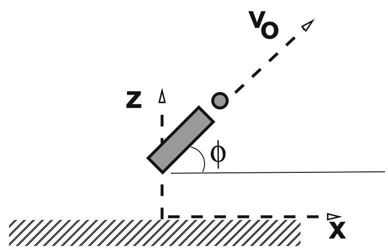

Fig. 2 Model problem for analytical study

S values larger than unity indicate that the situation is potentially unsafe.

3.5 Trends

In order to illustrate the behavior of this model, we consider (Fig. 2):

- The starting height, 1 m,
- Detonation energy, $E = 1$ Joule (TNT $= 4.6 \times 10^6$ Joules/kg),
- Density of air, $\rho_a = 1.225$, kg/m^3,
- Number of fragments, $N = 1000$,
- Density of detonation material, $\rho = 5000\,\text{kg/m}^3$,
- Total mass, $M = \sum_{i=1}^{N} m_i = 0.05\,\text{kg}$,
- Fragment masses, $m_i = (M/N)(1 + A_i)$, where $-0.95 \leq A_i \leq 0.95$,
- Heat capacity of $C = 1900$ J/^{o}K $-$ kg,
- Initial temperature $\theta(t = 0) = 1500$ K and
- Initial temperature $\theta^{safe} = 350$ K.

The convection coefficient (h) was generated using classical relations presented later (Eqs. 4.6–4.9). Figures 3 and 4 illustrate the results. In order to explain the results more qualitatively, consider the special case of $r_{iz}(0) = r_{iz}^{min}$, leading to

$$S = \frac{t^{safe}}{t^{tot}} = -\frac{m_i C_i g}{2h_i A_i^s v_{iz}(0)} Ln\left(\frac{\theta^{safe} - \theta_e}{\theta_i(0) - \theta_e}\right). \tag{3.20}$$

Utilizing $m_i = \rho_i \frac{4}{3}\pi R_i^3$ and $A_i = 4\pi R_i^2$ yields

$$S = \frac{t^{safe}}{t^{tot}} = -\frac{\rho_i C_i g R_i}{6h_i v_{iz}(0)} Ln\left(\frac{\theta^{safe} - \theta_e}{\theta_i(0) - \theta_e}\right). \tag{3.21}$$

The trends are:

- S grows (less safe) with particle size,
- S grows with (less safe) with larger initial temperature,
- S grows with (less safe) with larger density and heat capacity,
- S shrinks (more safe) with larger vertical initial velocity (longer loft time) and
- S shrinks with (more safe) with larger convection coefficients.

The total blast diameter was on the order of 10 m, and virtually all of the material that impacts the ground is hot enough to be dangerous. In order to add more physical features, such as nonlinear drag effects and radiative cooling, one must resort to some simple numerical methods, which we describe next.

4 Rapid numerical methods

The equation of motion for the ith fragment in the system is

$$m_i \dot{\boldsymbol{v}}_i = \boldsymbol{\Psi}_i^{tot} = \boldsymbol{\Psi}_i^{grav} + \boldsymbol{\Psi}_i^{drag} \tag{4.1}$$

where for the drag, we will employ a general phenomenological model

$$\boldsymbol{\Psi}_i^{drag} = \frac{1}{2}\rho_a C_D ||\boldsymbol{v}^f - \boldsymbol{v}_i||(\boldsymbol{v}^f - \boldsymbol{v}_i)A_i, \tag{4.2}$$

where C_D is the drag coefficient, A_i is the reference area, which for a sphere is $A_i = \pi R_i^2$, the surrounding fluid density is ρ_a (in the case of interest, air) and $\boldsymbol{v}^f$ is the surrounding velocity. The inner-product of the drag force with the relative velocity of the fragment to the surrounding environment provides the drag-heating rate, thus

$$\begin{aligned} m_i C_i \dot{\theta} &= \gamma \boldsymbol{\Psi}_i^{drag} \cdot (\boldsymbol{v}^f - \boldsymbol{v}_i) \\ &= \gamma \frac{1}{2}\rho_a C_D ||\boldsymbol{v}^f - \boldsymbol{v}_i||(\boldsymbol{v}^f - \boldsymbol{v}_i)A_i \cdot (\boldsymbol{v}^f - \boldsymbol{v}_i) \\ &= \gamma \frac{1}{2}\rho_a C_D ||\boldsymbol{v}^f - \boldsymbol{v}_i||^3 A_i, \end{aligned} \tag{4.3}$$

where $0 \leq \gamma \leq 1$ is the frictional heating efficiency. If one then includes convective and radiative cooling, this yields

$$\begin{aligned} m_i C_i \dot{\theta} &= \gamma \frac{1}{2}\rho_a C_D ||\boldsymbol{v}^f - \boldsymbol{v}_i||^3 A_i \\ &\quad + h_i(\theta_e - \theta_i)A_i^s + \epsilon_i \mathcal{B}(\theta_e^4 - \theta_i^4)A_i^s, \end{aligned} \tag{4.4}$$

where $0 \leq \epsilon_i \leq 1$ is the radiative efficiency, $\mathcal{B} = 5.670367 \times 10^{-8}\,\text{W}\,\text{m}^{-2}\text{K}^{-4}$ is the Stefan–Boltzmann constant and $A_i^s = 4\pi R_i^2$ is the radiative surface area.

4.1 Representation of the drag coefficient

To accurately account for the effects of drag, we employ an empirical drag coefficient that varies with Reynolds number (Chow [29]):

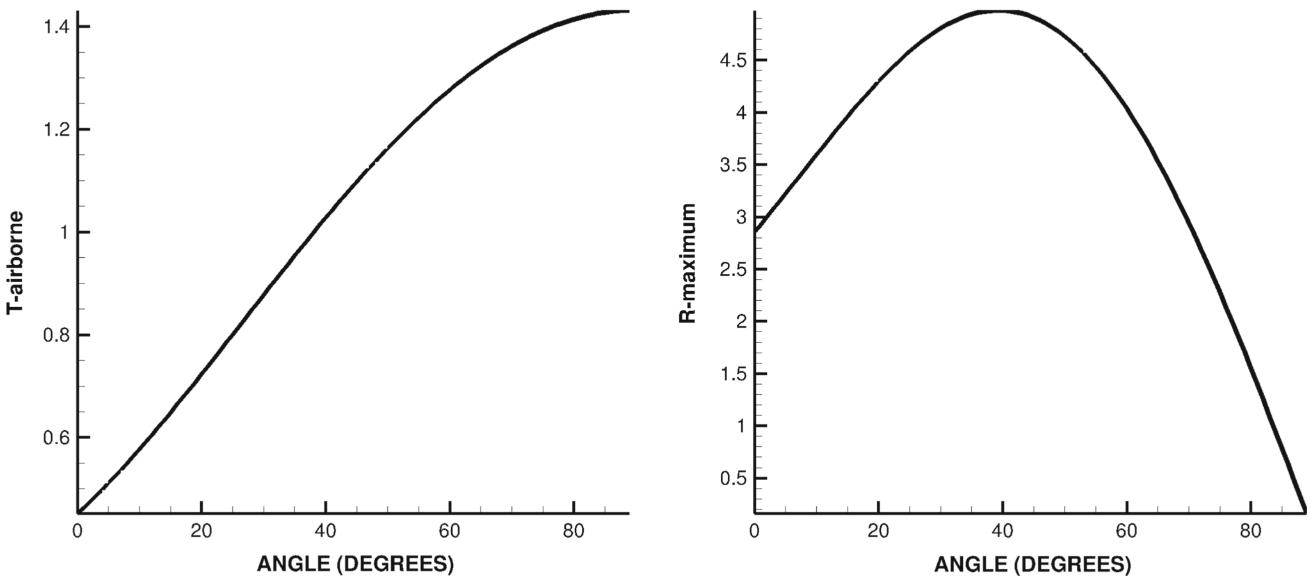

Fig. 3 Left Time airborne (s) as a function of launching angle $0 \leq \phi \leq \pi/2$, where $v_x = v_o cos\phi$ and $v_z = v_o sin\phi$. Right Travel distance x-direction (m)

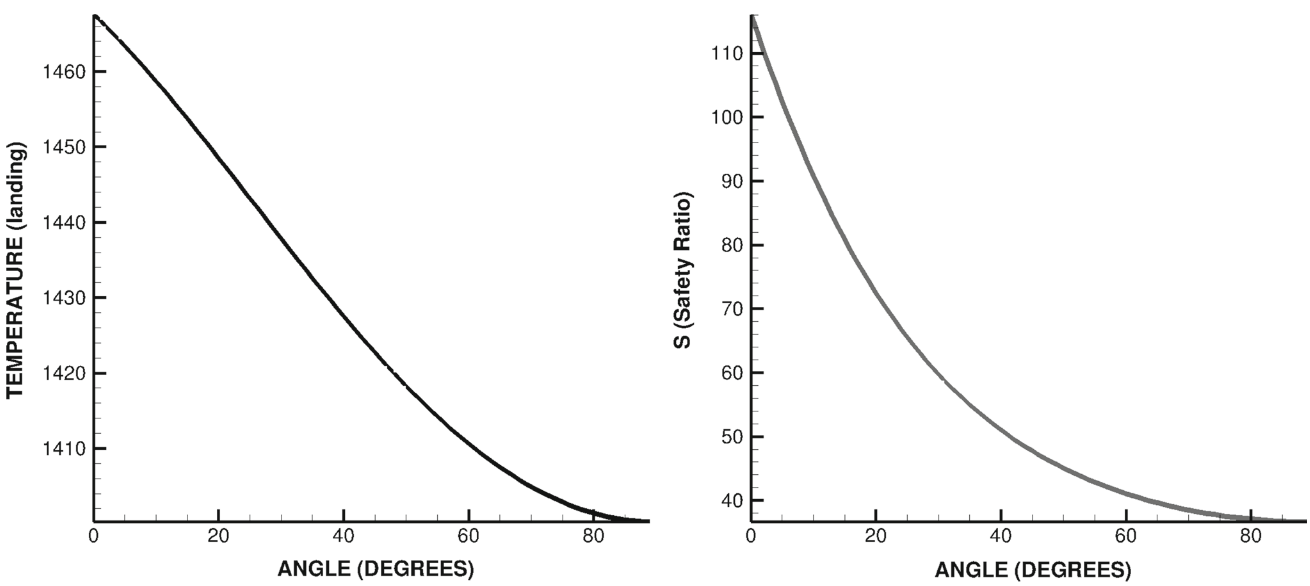

Fig. 4 Left Temperature at landing (K). Right $S \stackrel{\text{def}}{=} \frac{time\ to\ cool}{time\ airborne}$

- For $0 < Re \leq 1$, $C_D = \frac{24}{Re}$,
- For $1 < Re \leq 400$, $C_D = \frac{24}{Re^{0.646}}$,
- For $400 < Re \leq 3 \times 10^5$, $C_D = 0.5$,
- For $3 \times 10^5 < Re \leq 2 \times 10^6$, $C_D = 0.000366 Re^{0.4275}$,
- For $2 \times 10^6 < Re < \infty$, $C_D = 0.18$,

where the local Reynolds number for a fragment is $Re \stackrel{\text{def}}{=} \frac{2R\rho_a||\boldsymbol{v}^f - \boldsymbol{v}_i||}{\mu_f}$ and μ_f is the fluid viscosity.[2]

Remark This piecewise drag law is essentially a curve-fit of extensive data from Schlichting [30]. In the low Reynolds number limit, a Stokesian model is most appropriate-this is captured by the piecewise drag law since (Zohdi [51])

$$\begin{aligned} \boldsymbol{\Psi}_i^{drag,Stokesian} &= c(\boldsymbol{v}^f - \boldsymbol{v}_i) = \mu_f 6\pi R_i(\boldsymbol{v}^f - \boldsymbol{v}_i) \\ &= \frac{1}{2}\rho_a C_D ||\boldsymbol{v}^f - \boldsymbol{v}_i||(\boldsymbol{v}^f - \boldsymbol{v}_i)A_i = \boldsymbol{\Psi}_i^{drag} \end{aligned} \tag{4.5}$$

when $0 < Re \leq 1$, $C_D = \frac{24}{Re}$.

[2] The viscosity coefficient for air is $\mu_f = 0.000018$ Pa/s.

4.2 More accurate resolution of the heat transfer coefficient

To extend the constant convection coefficient to more realistic regimes, we consider the well-known heat transfer relation relating the Nusselt number, which is the ratio between the heat transfer of convection to heat transfer of conduction

$$Nu \stackrel{\text{def}}{=} \frac{hL}{K} \Rightarrow h\frac{NuK}{L}, \tag{4.6}$$

where h is the convection coefficient, $L = 2R$ is the length scale and K is the fluid conductivity, to the Reynolds number

$$Re \stackrel{\text{def}}{=} \frac{\rho 2R||\boldsymbol{v}^f - \boldsymbol{v}_i||}{\mu}, \tag{4.7}$$

and Prandtl numbers

$$Pr \stackrel{\text{def}}{=} \frac{c_p\mu}{K}, \tag{4.8}$$

which reads as (Whitaker [31])

$$Nu \approx 2 + (0.4Re^{1/2} + 0.06Re^{2/3})Pr^{0.4}\left(\frac{\mu}{\mu_s}\right)^{0.25}, \tag{4.9}$$

where μ is the surrounding fluid viscosity and μ_s is the viscosity of the fluid at the surface. In the analysis to follow, we assume $\mu_s \approx \mu$.

4.3 System discretization

The governing equation, with variable drag and gravity included is

$$\begin{aligned} m_i\dot{\boldsymbol{v}}_i &= \boldsymbol{\Psi}_i^{drag} + \boldsymbol{\Psi}_i^{grav} \\ &= \frac{1}{2}\rho_a C_D||\boldsymbol{v}^f - \boldsymbol{v}_i||(\boldsymbol{v}^f - \boldsymbol{v}_i)A_i + m_i\boldsymbol{g}, \end{aligned} \tag{4.10}$$

which we must integrate the governing equations numerically, using an explicit Euler scheme:

$$\begin{aligned} \boldsymbol{v}_i(t+\Delta t) &= \boldsymbol{v}_i(t) + \frac{1}{m}\int_t^{t+\Delta t} (\boldsymbol{\Psi}_i^{drag} + \boldsymbol{\Psi}_i^{grav})\,dt \\ &\approx \boldsymbol{v}_i(t) + \frac{\Delta t}{m_i}\left(\boldsymbol{\Psi}_i^{drag}(t) + \boldsymbol{\Psi}_i^{grav}(t)\right). \end{aligned} \tag{4.11}$$

For the temperature

$$\begin{aligned} \theta_i(t+\Delta t) &= \theta_i(t) + \frac{1}{m_iC_i}\int_t^{t+\Delta t}\left(\frac{\gamma}{2}\rho_a C_D||\boldsymbol{v}^f - \boldsymbol{v}_i||^3 A_i \right.\\ &\quad \left. + h_i(\theta_e - \theta_i)A_i^s + \epsilon_i\mathcal{B}(\theta_e^4 - \theta_i^4)A_i^s\right) dt \\ &= \theta_i(t) + \frac{\Delta t}{m_iC_i}\left(\frac{\gamma}{2}\rho_a C_D A_i||\boldsymbol{v}^f - \boldsymbol{v}_i||^3 \right.\\ &\quad \left. + h_i(\theta_e - \theta_i)A_i^s + \epsilon_i\mathcal{B}(\theta_e^4 - \theta_i^4)A_i^s\right). \end{aligned} \tag{4.12}$$

The solution procedure is straightforward. At a given time step:

- STEP 1: Update the velocities

$$\boldsymbol{v}_i(t+\Delta t) = \boldsymbol{v}_i(t) + \frac{\Delta t}{m_i}\left(\boldsymbol{\Psi}_i^{drag}(t) + \boldsymbol{\Psi}_i^{grav}(t)\right) \tag{4.13}$$

  and positions

$$\boldsymbol{r}_i(t+\Delta t) = \boldsymbol{r}(t) + \boldsymbol{v}_i(t)\Delta t. \tag{4.14}$$

- STEP 2: Update the temperature from the energy balance yielding

$$\begin{aligned} \theta_i(t+\Delta t) &= \theta_i(t) + \frac{\Delta t}{m_iC_i}\left(\frac{1}{2}\gamma\rho_a C_D A_i||\boldsymbol{v}^f - \boldsymbol{v}_i||^3 \right.\\ &\quad \left. + h_i(\theta_e - \theta_i)A_i^s + \epsilon_i\mathcal{B}(\theta_e^4 - \theta_i^4)A_i^s\right). \end{aligned} \tag{4.15}$$

- STEP 3: Repeat STEPS 1–2 for each particle.
- STEP 4: Go to the next time-step.

4.4 Numerical example

In order to illustrate the model, the following simulation parameters were chosen:

- Total simulation duration, 1.5 s,
- The time step size, $\Delta t = 10^{-4}$ s,
- The starting height, 1 m,
- Detonation energy, $E = 1$ Joule (TNT $= 4.6 \times 10^6$ Joules/kg),
- Density of air, $\rho_a = 1.225$, kg/m^3,
- Number of fragments, $N = 1000$,
- Density of detonation material, $\rho = 1000$ kg/m^3,
- Total mass, $M = \sum_{i=1}^{N} m_i = 0.05$ kg,
- Fragment masses, $m_i = (M/N)(1 + A_i)$, where $-0.95 \leq A_i \leq 0.95$,
- Environmental surrounding's velocity profile: $\boldsymbol{v}_f = (0, 10z, 0)$ m/s,

- Frictional heating efficiency, $\gamma = 1$,
- Heat capacity of $C = 1900$ J/^{o}K − kg and
- Radiative efficiency, $\epsilon = 0.5$,
- Initial temperature $\theta(t = 0) = 1500$ K.

As before, the convection coefficient (h) was generated using Eqs. 4.6–4.9. The fragments were initially randomly distributed in a spherical domain that was one meter above the ground. The initial spherical domain radius was computed from

$$R_o = \left(\frac{M}{\frac{4}{3}\rho\pi}\right)^{\frac{1}{3}}. \tag{4.16}$$

For the parameters chosen, $R_o = 0.0133$ m. An extremely small time-step size (relative to the total simulation time) of $\Delta t = 10^{-4}$ s was used. Reducing the time-step size below the value used produced no noticeable changes in the results, thus one may assume that the solutions generated contain negligible numerical error. The simulations took under 2 s on a standard laptop. For the chosen parameters, Fig. 5 illustrates the results. Note that the temperature downstream (aligned with the wind current) is higher than upstream (against the wind current), since the relative velocity is smaller downstream than upstream, and thus cools less due to convection. These parameters yielded a blast radius of slightly larger than 4 m in the lateral directions, 10 m in the downwind direction and slightly less than 2 m upwind. Thus, the total blast diameter was on the order of 12 m, skewed in the wind direction and 8 m in the lateral (non-wind) direction, as opposed to approximately 10 m circular distribution in the drag free analytical results. The results also indicate that radiation's effects are thermally-inconsequential, due to the short time-scales. However, as Fig. 5 clearly indicates, that while the temperature decreases radially, virtually all of the material that impacts the ground is hot enough to be dangerous-again in agreement with the analytical safety ratio calculations. The selection of $\gamma = 1$ was the maximum possible frictional heating. However, it turns out that the heating that the parameter multiplies is insignificant in the velocity range calculated (extremely high velocities are needed). In hindsight, the observed trends are understandable because:

- The key force ratio is

$$\frac{drag\ force}{gravitational\ force} = \frac{||\boldsymbol{\Psi}_i^{drag}||}{||\boldsymbol{\Psi}_i^{grav}||} = \frac{\frac{1}{2}\rho_a C_D ||\boldsymbol{v}^f - \boldsymbol{v}_i||^2 A_i}{m_i g} = \frac{3\rho_a C_D ||\boldsymbol{v}^f - \boldsymbol{v}_i||^2}{8\rho_i R_i g}, \tag{4.17}$$

which indicates that drag can play a significant role in the dynamics.

- The key thermal ratios are

$$\frac{atmospheric\ heating}{convective\ cooling} = \frac{\gamma\rho_a C_D A_i ||\boldsymbol{v}^f - \boldsymbol{v}_i||^3}{2h(\theta_e - \theta_i)A_i^s} = \frac{\gamma\rho_a C_D ||\boldsymbol{v}^f - \boldsymbol{v}_i||^3}{8h(\theta_e - \theta_i)} \tag{4.18}$$

and

$$\frac{radiative\ cooling}{convective\ cooling} = \frac{\epsilon\mathcal{B}(\theta_e^4 - \theta_i^4)A_i^s}{h(\theta_e - \theta_i)A_i^s} = \frac{\epsilon\mathcal{B}(\theta_e^4 - \theta_i^4)}{h(\theta_e - \theta_i)} \tag{4.19}$$

which for the parameters in this problem are extremely small-convection dominates.

Remark Note that any buoyancy forces (not included in this analysis) would scale as

$$\frac{buoyancy\ force}{gravitational\ force} = \frac{||\boldsymbol{\Psi}_i^{buo}||}{||\boldsymbol{\Psi}_i^{grav}||} = \frac{\rho_a}{\rho_i} \tag{4.20}$$

which are rather small.

5 Summary

In summary, this paper, developed mathematical models to characterize the progressive time-evolution of a fragmenting incandescent object, with the objective being to objective provide a spatio-thermal footprint of the fragmentation field, which can be useful to guide fire safety rules in manufacturing workplaces, etc. Because of the difficulty of ascertaining the time-evolution of the temperature of the fragments experimentally, a direct numerical scheme based on particle dynamics was constructed, which uses the released energy from the initial blast pulse to provide the starting kinetic energy of the system of particles and then numerically computes the trajectory and thermal state of the fragments under the influence of (a) drag from the surrounding air, (b) gravitational settling and (c) convective and radiative cooling. Analytical models based solely on ballistics, were first developed to provide qualitative trends, identifying key fundamental ratios that govern safe areas in a spatio-thermal map. Thereafter, rapid numerical spatio-thermal models, which provide quantitative information, were then developed. A full-scale simulation take under 2 seconds-making it ideal for parameter studies.

In closing, we emphasize that the analysis presented can be used to analyze cases where the ejecta may contain hazardous and even biohazardous material, where it is important

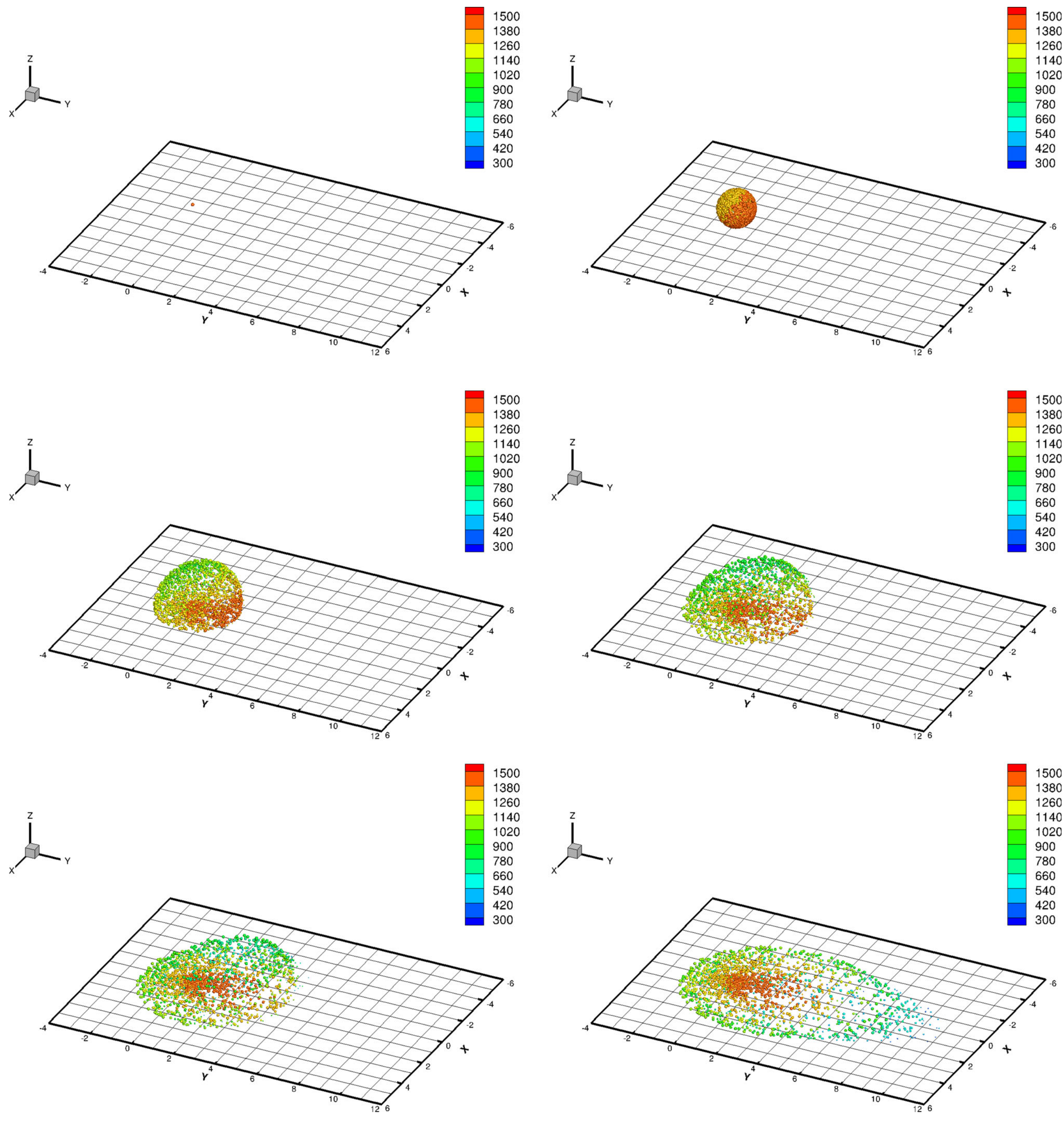

Fig. 5 Simulation with random fragment masses, $m_i = (M/N)(1 + A_i)$, where $-0.95 \leq A_i \leq 0.95$, with detonation energy of one Joule and mass of 0.05 kg (colors indicate temperature). This yielded a blast radius of slightly larger than 4 m in the lateral directions, 10 m in the downwind direction and slightly less than 2 m upwind. *NOTE* The fragments were initially randomly distributed in a small spherical domain that was 1 m above the ground. The initial spherical domain radius was computed from Eq. 4.16. For the parameters chosen, $R_o = 0.0133$ m. The simulation represents successive 0.2 s snapshots. (Color figure online)

to have a fast computational tool, especially with respect to emergency management and to limit of human exposure. In Zohdi and Cabalo [54], a systematic study of an explosive device was considered combining the results from a set full scale field experiments with high explosives and ballistic gelatin and reduced order models, similar to those presented in this paper, neglecting the interaction between the shock wave and the packed fragments and any chemical aspects.[3] There were extremely close matches between experiments and numerics, indicating that it is likely that a drag-based particle noninteraction model is appropriate.[4] There can be cases where the surrounding fluid's behavior can be affected by the fragments. With those cases in mind, had the fragment noninteraction approximation not been invoked, a coupled system of equations would arise

$$\begin{aligned} \boldsymbol{v}_i(t+\Delta t) &= \boldsymbol{v}_i(t) + \frac{1}{m_i}\int_t^{t+\Delta t}\left(\boldsymbol{\Psi}_i^{grav} + \sum_{j=1, j\neq i}^{K}\boldsymbol{\Psi}_{ij} + \boldsymbol{\Psi}_i^{fluid}\right) dt \\ &\approx \boldsymbol{v}_i(t) + \frac{\Delta t\phi}{m_i}\left(\boldsymbol{\Psi}_i^{grav}(t+\Delta t)\right. \\ &\quad \left. + \sum_{j=1, j\neq i}^{K}\boldsymbol{\Psi}_{ij}(t+\Delta t) + \boldsymbol{\Psi}_i^{fluid}(t+\Delta t)\right) \\ &\quad + \frac{\Delta t(1-\phi)}{m_i}\left(\boldsymbol{\Psi}_i^{grav}(t) + \sum_{j=1, j\neq i}^{N}\boldsymbol{\Psi}_{ij}(t) + \boldsymbol{\Psi}_i^{fluid}(t)\right), \end{aligned} \tag{5.1}$$

where an implicit trapezoidal rule with variable integration metric ($0 \leq \phi \leq 1$) has been used and where $\boldsymbol{\Psi}_i^{fluid}$ represents the interaction of fragment i with the fluid and $\boldsymbol{\Psi}_{ij}(t)$ represents its interaction with the neighboring $j = 1, 2, \ldots N$ fragments. The position can be computed as

$$\boldsymbol{r}_i(t+\Delta t) \approx \boldsymbol{r}_i(t) + \Delta t(\phi\boldsymbol{v}_i(t+\Delta t) + (1-\phi)\boldsymbol{v}_i(t)), \tag{5.2}$$

which can be consolidated into

$$\begin{aligned} \boldsymbol{r}_i(t+\Delta t) &= \boldsymbol{r}_i(t) + \boldsymbol{v}_i(t)\Delta t + \frac{\phi^2(\Delta t)^2}{m_i} \\ &\times \left(\boldsymbol{\Psi}_i^{grav}(t+\Delta t) + \sum_{j=1, j\neq i}^{N}\boldsymbol{\Psi}_{ij}(t+\Delta t) + \boldsymbol{\Psi}_i^{fluid}(t+\Delta t)\right) \\ &+ \frac{\phi(1-\phi)(\Delta t)^2}{m_i}\left(\boldsymbol{\Psi}_i^{grav}(t) + \sum_{j=1, j\neq i}^{K}\boldsymbol{\Psi}_{ij}(t) + \boldsymbol{\Psi}_i^{fluid}(t)\right). \end{aligned} \tag{5.3}$$

A coupled system of equations arise for the interaction between the fragments and the fluid, which would necessitate spatio-temporal discretization using, for example Finite Element, Finite Difference, Finite Volume or Discrete Element Methods (Onate et al. [39,40], Avci and Wriggers [41], Leonardi et al. [42], Onate et al. [44], Bolintineanu et al. [43] and Zohdi [45–50]). Furthermore, advanced models should also involve detailed modeling of the initial fragmentation of the material (Zohdi [52,53]), coupled to the evolution of heat and surrounding fluid mechanics environment. This is under current investigation by the author.

[3] For shock analyses, see, for example, Hoover and Hoover [32], Gregoire et al. [33], Kudryashova et al. [34] and Cabalo et al. [35,36].

[4] One conclusion from these experiments is that aerosols generated from a blast containing toxic materials cannot be assumed to be inactivated by the blast itself, which is consistent with findings of Eshkol and Katz [37] and Kanemitsu [38], where Hepatitis B from a suicide bomber was transmitted to survivors of the blast.

References

1. Wingerden VK, Hesby I, Eckhoff R (2011) Ignition of dust layers by mechanical sparks. In: Proceedings of 7th global congress on process safety, Chicago, Ill
2. Fernandez-Pello AC (2017) Wildland fire spot ignition by sparks and firebrands. Fire Saf J 91:2–10
3. National Interagency Fire Center. www.nifc.gov/fireInfo/nfn.htm
4. Prestemon JP, Hawbaker TJ, Bowden M, Carpenter J, Brooks MT, Abt KL, Sutphen R, Scranton S (2013) Wildfire ignitions: a review of the science and recommendations for empirical modeling (technical report). US Department of Agriculture: Forest Service, Asheville
5. Ahrens M (2013) Brush, grass and forest fires (technical report). National Fire Protection Association, Quincy
6. Ramljak I, Majstrovic M, Sutloviec S (2014) Statistical analysis of particles of conductor clashing. Dubrovnic May 13–16
7. National Fire Protection Association (2014) NFPA 51B: standard for fire prevention during welding, cutting and other hot work
8. US Fire Administration. http://www.usfa.fema.gov/statistics/estimates/wildfire.shtm
9. Pleasance GE, Hart JA (1977) An examination of particles from conductors clashing as possible source of bushfire ignition. State Electricity Commission of Victoria (SEC), Victoria, Australia, Research and Development Department, Report FM-1
10. Stokes AD (1990) Fire ignition by copper particles of controlled size. J Electr Electron Eng Aust 10:188–194
11. Rowntree G, Stokes A (1994) Fire ignition of aluminum particles of controlled size. J Electr Electron Eng 117–123
12. Hadden R, Scott S, Lautenberger C, Fernandez-Pello CA (2011) Ignition of combustible fuel beds by hot particles: an experimental and theoretical study. Fire Technol 47:341–355
13. Urban JL, Zak CD, Song J, Fernandez-Pello AC (2017) Smolder spot ignition of natural fuels by a hot metal particle. Proc Combust Inst 36(2):3211–3218. ISSN 1540-7489. https://doi.org/10.1016/j.proci.2016.09.014
14. Baum HR, McCaffrey BJ (1989) Fire induced flow field-theory and experiments fire safety science. In: Wakamatsu et al. (eds) Proceedings of the second international symposium. Washington DC, pp 129–148
15. Tarifa CS, del Notario PP, Moreno FG (1965) On the flight paths and lifetimes of burning particles of wood. Proc Combust Inst 10:1021–1037
16. Tarifa CS, Del Notario PP, Moreno FG, Villa AR (1967) Transport and combustion of firebrands. U.S. Department of Agriculture Forest Service (Final Report of Grants GF-SP-114 and GF-SP-146. Madrid, May)
17. Sardoy N, Consalvi JL, Poterie B, Loraud JC, Fernandez-Pello CA (2007) Modeling transport and combustion of firebrands from burning trees. Combust Flame 150:151–169
18. Lee SL, Hellman JM (1970) Firebrand trajectory study using an empirical velocitydependent burning law. Combust Flame 15:265–274
19. Koo E, Pagni P, Linn R (2007) Using FIRETEC to describe firebrand behavior in wildfires, fire mater. 2007 San Francisco, CA
20. Tse SD, Fernandez-Pello AC (2006) On the flight paths of metal particles and embers generated by powerlines in high winds—a potential source of wildland fires. Fire Saf J 333–356

21. Mills FA, Hang X (1984) Trajectories of sparks from arcing aluminum power cables. Fire Technol 20:5–14
22. Rallis CJ, Mangaya BM (2002) Ignition of veld grass by hot aluminum particles ejected from clashing overhead transmission lines. Fire Technol 38:81–92
23. Russell BD, Benner CI, Wischkaemper JA (2012) Distribution feeder caused wildfires: mechanisms and prevention. Prot Relay Eng 43
24. Blackburn T (1985) Conductor clashing characteristics of overhead lines. In: Proceedings of electrical energy conferences. p 202
25. Pagni PJ (1993) Causes of the 20 October 1991 Oakland-hills conflagration. Fire Saf J 21:331–339
26. Gilbert M California Department of Forestry and Fire Protection Investigation Report: Incident number 07- CA-MVU-10432. http://www.fire.ca.gov/fire
27. Maranghides A, Mell W (2009) A Case Study of a Community Affected by the Witch and Guejito Fires, NIST Technical Note 1635. http://fire.nist.gov/bfrlpubs/fire09/art028.html
28. Badger S (2012) Large-loss fires in the United States 2011. National Fire Protection Association, Quincy
29. Chow CY (1980) An introduction to computational fluid dynamics. Wiley, New York
30. Schlichtling H (1979) Boundary-layer theory, 7th edn. McGraw-Hill, New York
31. Whitaker S (1972) Forced convection heat transfer correlations for flow in pipes, past flat plates, single cylinders, single spheres, and flow in packed beds and tube bundles. AIChE J 18:361–371
32. Hoover WG, Hoover CG (2009) Tensor temperature and shock-wave stability in a strong two-dimensional shock wave. Phys Rev E Stat Nonlinear Soft Matter Phys 80:011128/1–011128/6
33. Gregoire Y, Sturtzer M-O, Khasainov BA, Veyssiere B (2009) Investigation of the behavior of solid particles dispersed by high explosive. In: Int annu conf ICT 40th, 35/1–35/12
34. Kudryashova OB, Vorozhtsov BI, Muravlev EV, Akhmadeev IR, Pavlenko AA, Titov SS (2011) Physicomathematical modeling of explosive dispersion of liquid and powders, propellants, explos. Pyrotechnology 36:524–530
35. Cabalo J, Schmidt J, Wendt JOL, Scheeline A (2002) Spectrometric system for characterizing drop and powder trajectories and chemistry in reactive flows. Appl Spectrosc 56:1346–1353
36. Cabalo JB, Kesavan J, Sickenberger DW, Diviacchi G, Maldonado-Figueroa C, McGrady D, Stafford K (2016) Assessing the biological threat posed by suicide bombers. Report ECBC-TR-1363
37. Eshkol Z, Katz K (2005) Injuries from biologic material of suicide bombers. Injury 36:271–274
38. Kanemitsu K (2005) Does incineration turn infectious waste aseptic? J Hosp Infect 60(4):304–306
39. Onate E, Idelsohn SR, Celigueta MA, Rossi R (2008) Advances in the particle finite element method for the analysis of fluid-multibody interaction and bed erosion in free surface flows. Comput Methods Appl Mech Eng 197(19–20):1777–1800
40. Onate E, Celigueta MA, Idelsohn SR, Salazar F, Surez B (2011) Possibilities of the particle finite element method for fluid-soil-structure interaction problems. Comput Mech 48:307–318
41. Avci B, Wriggers P (2012) A DEM-FEM coupling approach for the direct numerical simulation of 3D particulate flows. J Appl Mech 79:010901-1–7
42. Leonardi A, Wittel FK, Mendoza M, Herrmann HJ (2014) Coupled DEM-LBM method for the free-surface simulation of heterogeneous suspensions. Comput Particle Mech 1(1):3–13
43. Bolintineanu DS, Grest GS, Lechman JB, Pierce F, SJ Plimpton, PR Schunk (2014) Particle dynamics modeling methods for colloid suspensions. Comput Particle Mech 1(3):321–356
44. Onate E, Celigueta MA, Latorre S, Casas G, Rossi R, Rojek J (2014) Lagrangian analysis of multiscale particulate flows with the particle finite element method. Comput Particle Mech 1(1):85–102
45. Zohdi TI (2004) A computational framework for agglomeration in thermo-chemically reacting granular flows. Proc R Soc 460(2052):3421–3445
46. Zohdi TI (2007) Computation of strongly coupled multifield interaction in particle-fluid systems. Comput Methods Appl Mech Eng 196:3927–3950
47. Zohdi TI (2010) On the dynamics of charged electromagnetic particulate jets. Arch Comput Methods Eng 17(2):109–135
48. Zohdi TI (2013) Numerical simulation of charged particulate cluster-droplet impact on electrified surfaces. J Comput Phys 233:509–526
49. Zohdi TI (2014) Additive particle deposition and selective laser processing—a computational manufacturing framework. Comput Mech 54:171–191
50. Zohdi TI (2014) Mechanically-driven accumulation of microscale material at coupled solid-fluid interfaces in biological channels. Proc R Soc Interface 11:20130922
51. Zohdi TI (2016) A note on firework blasts and qualitative parameter dependency. Proc R Soc. https://doi.org/10.1098/rspa.2015.0720
52. Zohdi TI (2003) Genetic design of solids possessing a random-particulate microstructure. Philos Trans R Soc Math Phys Eng Sci 361(1806):1021–1043
53. Zohdi TI (2003) On the compaction of cohesive hyperelastic granules at finite strains. Proc R Soc 454(2034):1395–1401
54. Zohdi TI, Cabalo J (2017) On the thermomechanics and footprint of fragmenting blasts. Int J Eng Sci 118:28–39